ELSEVIER

Journal of Quantitative Spectroscopy & Radiative Transfer 100 (2006) 315–324

Journal of Quantitative Spectroscopy & Radiative Transfer

www.elsevier.com/locate/jqsrt

Light-scattering methods for modelling algal particles as a collection of coated and/or nonspherical scatterers

Arturo Quirantes[a,*], Stewart Bernard[b]

[a]*Departamento de Física Aplicada, Facultad de Ciencias, Universidad de Granada, 18071 Granada, Spain*
[b]*Department of Oceanography, University of Cape Town, Private Bag, Rondebosch 7700 Cape Town, South Africa*

Abstract

Ocean reflectance or ocean colour measurements are an important tool for oceanographic studies of phytoplankton dynamics. Theoretical models based on homogeneous, spherical particles underestimate algal backscattering and thus reflectance values. It is our understanding that more advanced light-scattering methods must be employed, both for refractive index retrieval (Mie, Aden–Kerker) with inverse models, and for backscattering calculations (Extended Boundary Condition Method, EBCM). The measured optical properties of a monospecific bloom of the marine brown tide pelagophyte *Aureococcus anophagefferens* are used to compare the effects of assuming various simulated particle geometries. Computational results from polydisperse, coated spherical particles show results that compare better to experimental reflectance values than calculations based on homogeneous spheres. No noticeable change in simulated reflectance values is observed when a randomly oriented coated spheroidal (rather than spherical) geometry is assumed for the particle population. Our results suggest that a layered spherical geometry, based on Aden–Kerker theory, can adequately reproduce experimentally determined light-scattering properties even supposedly shape-sensitive properties such as the backscattering coefficient.

Keywords: Light-scattering; EBCM; Nonspherical particles; Algae

1. Introduction

Characterising the scattering and absorbing properties of algal populations is essential to the effective use of ocean colour and other bio-optical tools used for the measurement of algal dynamics. Such tools have important application in the analysis of global carbon cycles and coastal ecological management, of which a specific example is the monitoring and detection of harmful algal blooms. The equations of radiative transfer typically rely on a correct description of particulate inherent optical properties (IOPs) in order to describe the propagation of light through the sea [1]. The radiant flux emerging from the sea surface is therefore determined by the spectral nature of the volume scattering and absorption coefficients. Ocean colour can be parameterised in the form $R \propto b_b/(a + b_b)$, where R is the reflectance, b_b is the backscattering coefficient and a

*Corresponding author.
E-mail addresses: aquiran@ugr.es (A. Quirantes), bstewart@ocean.uct.ac.za (S. Bernard).

0022-4073/$ - see front matter © 2005 Elsevier Ltd. All rights reserved.
doi:10.1016/j.jqsrt.2005.11.048

is the absorption coefficient [2]. Understanding the contribution of algal cells to the absorption and backscattering coefficients (the integrated angular scattering that is responsible for returning light to the surface of the sea) can be seen to be crucial to ocean colour studies.

While algal absorption is relatively easy to measure directly, measurements of angular scattering are methodologically difficult. Theoretical models have provided an alternative to direct measurement, and in addition, offer the capacity for a holistic description of all particulate IOPs. The current understanding of algal scattering properties is largely based on Mie theory [3,4], and the related anomalous diffraction approximation (ADA) [5]. The reasons for the adoption of Mie or ADA modelling are based in simplicity of implementation and use. However, the assumption of spherical homogeneity is a potential shortcoming with regard to algal cells, where scattering particles are neither homogeneous nor spherical. The few direct measurements made of algal angular scattering suggest that Mie theory is not well suited to simulate backward scattering [6,7]; both internal structure and nonsphericity may exert considerable influence on algal scattering in the backward direction [8].

The present work demonstrates the application of several currently available light-scattering theories to describing the optical properties of a bloom of the small brown tide pelagophyte *Aureococcus anophagefferens*. Absorption and size distribution measurements made on the natural algal population are used to derive appropriate complex refractive index data, using both a homogeneous and a two-layered spherical geometry. The latter geometry is chosen as the simplest heterogeneous structure that has shown itself capable of reproducing algal angular scattering properties [6], and the suitability of the various equivalent cell structures available with this geometry are discussed. Refractive index spectra are then used to calculate IOPs for four particle geometries: homogeneous spheres (Mie theory), two-layered spheres (Aden–Kerker theory), and homogeneous and two-layered spheroids (Extended Boundary Condition Method, EBCM). Geometry-associated effects on ocean colour were considered using the reflectance approximation [2]: simulated reflectance spectra are compared to reflectance measurements of the sample water body made with a hyperspectral radiometer. The validity of the different geometries are assessed with regard to refractive index derivations, IOP modelling and the resultant effects on ocean colour.

2. Materials

2.1. Measurements

Measurements were made on a bloom of the pelagophyte *Aureococcus anophagefferens* that occurred in a small salt water dam in Saldanha Bay, South Africa in January 2004. The bloom was determined to be mono-specific by microscopic analysis, and imparted a golden-brown colour to the water.

Particulate absorption data were measured with the quantitative filter pad technique [9,10] using GF/F filters and a Shimadzu UV-2501 spectrophotometer equipped with a ISR-2200 internal integrating sphere. Absorption coefficients were calculated using the pathlength amplification factor of Roesler [10] assuming a null point correction at 750 nm. Detrital measurements were made using methanol extraction on the filter, followed by re-reading in the spectrophotometer [11]. Phytoplankton absorption $a_\phi(\lambda)$ data were then obtained by subtraction of detrital absorption $a_d(\lambda)$ from total particulate absorption $a_p(\lambda)$.

Particle size distribution (PSD) measurements were made using a 128 channel Coulter Multisizer II with a 50 μm using freshly prepared 0.2 μm filtered seawater as both blank and electrolyte. A numerical technique was employed to fractionate measured size distributions into algal and non-algal components, designed to produce data analogous to the phytoplankton absorption data fractionated using the methods of Kishino et al. [11]. Briefly, the detrital distribution is calculated from fitting an exponential size distribution to measured detrital absorption $a_d(\lambda)$ using an assumed imaginary refractive index [4] and an inverse anomalous diffraction (IAD) model. The detrital size distribution resulting from the fit was then subtracted from the total measured size distribution to obtain the algal particle size distribution. Final PSD data were resampled to 0.1 μm size resolution through calculation of the spectral density.

Remote sensing reflectance measurements were derived from measurements of in-water upwelling radiance L_u and above surface downwelling irradiance E_d, made with a Satlantic Hyperspectral Tethered Surface Radiometer Buoy (H-TSRB). The instrument provides radiometric data with a spectral range of 400–800 nm

at a spectral resolution of 3.3 nm. Upwelling radiance spectra were measured at a nominal depth of 0.66 m—these data were propagated to the surface and remote sensing reflectance R_{rs} derived using the conventions of Albert and Mobley [12].

Additional bio-optical measurements were made with a WetLabs AC-9 (a nine wavelength absorption and attenuation meter) to determine the absorbing and scattering values of the particulate and dissolved component. Unaltered samples and the GF/F filtrate were run through the AC-9 in a benchtop mode to obtain spectral absorption and attenuation data—three replicate samples were processed according to the manufacturers convention [13] and averaged.

2.2. Refractive index determinations

Refractive index (RI) spectra were then obtained using the derived algal absorption and size distribution data, several assumptions concerning cellular morphology and RI ranges based on previously published data, and inverse anomalous diffraction, Mie and Aden–Kerker models. A two-layered geometry was assumed for heterogeneous geometry calculations, based on a peripheral chloroplast layer location (see later Section 4) with a relative volume of 15% (based on transmittance electron micrographs of *A. anophagefferens*). Spectra of the real part of the RI $n(\lambda)$, whether for homogeneous cells or heterogeneous cell layers, were calculated by application of the Kramers–Kronig (KK) relations to the imaginary part of the RI $n'(\lambda)$, with the magnitude of n fixed around a chosen central value $1+\varepsilon$ [14]. In practice the KK relations can be calculated as the imaginary part of a Hilbert transform. RI determinations were made as follows:

1. Experimental algal absorption efficiency factors Q_a were calculated from algal absorption and size distribution data, and initial homogeneous imaginary RI spectra derived from these with an inverse anomalous diffraction model [3]. Initial values for subsequent inverse RI models were based on Gladstone–Dale equivalence of these initial IAD derived data. All subsequent RI determinations were based on matching these experimental Q_a data, using the full 0.1 μm resolution algal PSD.
2. A two-layered model [15] was run iteratively in an inverse mode to establish the imaginary RI of the chloroplast n'_{chlor}, calculating the real RI of the chloroplast n_{chlor} between successive runs with the KK relations. A cytoplasm imaginary RI of $n'_{cyto} = 5\times10^{-4}\exp(-0.01(\lambda-400))$ was assumed based on previously presented data regarding detrital and cellular optical properties [4,16]. Final central n values for chloroplast and cytoplasm were chosen based on both previously published values [17,18] and values needed to provide a good fit for the inverse model. These values were $1+\varepsilon = 1.035$ (cytoplasm) and $1+\varepsilon = 1.14$ (chloroplast). Cytoplasm real RI data n_{cyto} were also calculated with the KK relations from $n'_{cyto}(\lambda)$ values.
3. Homogeneous RI data were recalculated using a full Mie theory inverse model [15], calculating the real RI of the homogeneous cell n_{hom} between successive runs with the KK relations. This was done after finding that the homogeneous ADA-derived RI data resulted in an ~10% error when calculating modelled vs. measured absorption coefficients. A homogeneous central real RI value of $1+\varepsilon = 1.051$ was assumed, based on Gladstone–Dale volume equivalence of the two-layered RI values. It should be noted that this is the only volume equivalence between the homogeneous and heterogeneous particles—in all other senses they are "absorption equivalent".

Having established reasonable refractive index data, it is necessary to make a decision on whether it is more appropriate to model the chloroplast as the inner or outer core. In order to address this question, the package effect (PE) was calculated. The PE describes the consequence of placing the absorbing cellular material in particulate as opposed to solution form, and is the ratio of the particulate specific absorption $a^*(\lambda)$ to the specific absorption of the same material perfectly in solution $a^*_{sol}(\lambda)$: $Q^*_a = a^*/a^*_{sol}$. It can be assumed, from a general phycological cost-benefit perspective, than an algal cell will benefit from minimising absorption packaging. Direct measurements of absorption packaging indicate that packaging tends to be lower than predicted by theory, i.e. Q^*_a is close to one [19]. Given both factors, it would thus seem reasonable to adopt a model geometry that minimises packaging—the outer chloroplast model.

For a suspension of coated particles with radius r and outer size parameter $x = kr$, core/particle ratio q and indices of refraction $m_1 = n_1 + in'_1$ and $m_2 = n_2 + in'_2$ for core and shell, respectively, an expression is derived as

$$Q_a^* = \frac{3}{8}\frac{Q_a}{xn'_1q^3 + xn'_2(1-q^3)}. \tag{1}$$

Aden–Kerker [20] calculations were made for layered spheres of varying size and several core volume fractions (ranging from 5% to 30%). Refractive index values were taken as $1.12 + i0.02$ and $1.02 + i0.0005$ to represent chloroplast and cytoplasm, respectively. Fig. 1a shows the considerable difference in packaging between the inner and outer chloroplast models for a 20% chloroplast volume fraction. The inner model has Q_a^* values approximately up to 40% lower, meaning that the absorption packaging is approximately 40% higher; in comparison, the packaging of the homogeneous and outer layer model differ by a maximum of 10%. It is the difference in Q_a values that is the predominant cause of these packaging differences, as Fig. 1b show. In addition, reported experimental Q_a values considerably larger than 0.5 are not uncommon, while the

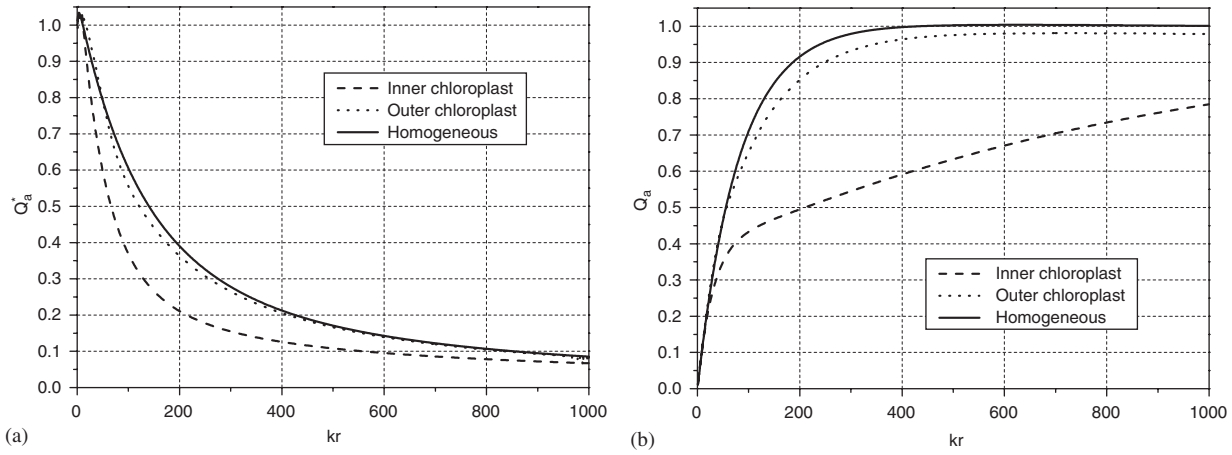

Fig. 1. (a) Package effect ratio Q_a^* and (b) absorption efficiency Q_a against size parameter kr for two-layered and homogeneous spheres. Two-layered spheres in both inner (dashed line) and outer (dotted line) chloroplast configurations have refractive indices of $m_{ch} = 1.12 + i0.02$ and $m_{cy} = 1.02 + i0.0005$. Homogeneous spheres (solid line) have a refractive index of $m_h = 1.04 + i0.0044$. Relative chloroplast volume is set to 20%.

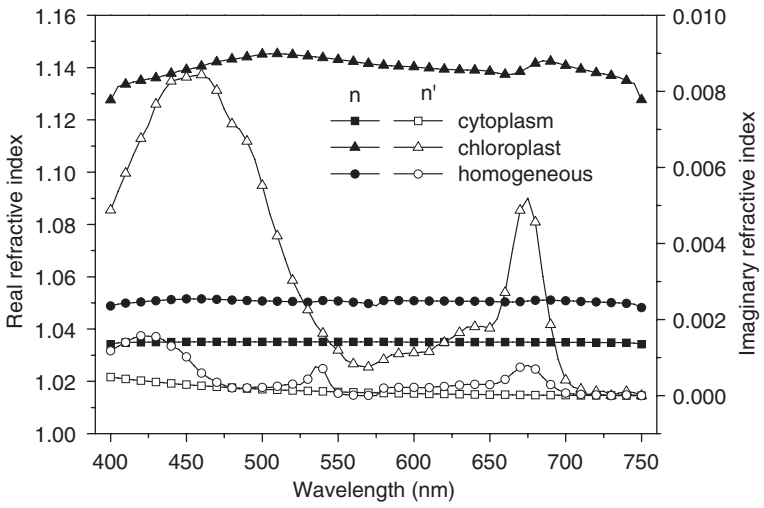

Fig. 2. Refractive index values $m = n + in'$ for cytoplasm (squares) and chloroplast (triangles), as well as for homogeneous particles (circles).

inner chloroplast model typically yields Q_a values smaller than 0.5, except for very large cells ($>30\,\mu m$ diameter). Finally, examination of transmittance electron micrographs from morphometrical studies confirm that, for a wide variety of species, chloroplasts are located peripherically.

It thus seems more reasonable to base our model on a two-layered geometry with a cytoplams core and a chloroplast shell. Fig. 2 shows the complex refractive index values for both cytoplasm (m_{cy}) and chloroplast (m_{ch}), as retrieved from absorption measurements under the assumption of a chloroplast outer layer with a relative volume $V_{ch} = 15\%$; homogeneous RI values are also shown.

3. Theory

Extinction, scattering, and absorption cross sections (C_{ext}, C_{sca}, C_{abs}) have been calculated by using the EBCM, for nonspherical particles [21,22] adapted for two-layer axisymmetric scatterers [23,24]. Coated prolate spheroids with axes a,b (a = revolution axis), eccentricity $\varepsilon = b/a$, and core/particle size parameter ratio q, are used. Data for spheres (both homogeneous and coated), and homogeneous spheroids, were also calculated for comparison purposes. Refractive index values used are those retrieved from absorption measurements and shown in Fig. 2. Cross sections were calculated to an accuracy of 10^{-6}, except for some cases ($\lambda < 510$ nm) where convergence problems were encountered for coated spheroids and only an accuracy of 10^{-5} was obtained.

In addition, the hemispheric backscattering probability factor (referred to here as the backscattering ratio), defined as

$$Q_{back} = \frac{\int_{\pi/2}^{\pi} F_{11}(\theta)\sin(\theta)\,d\theta}{\int_{0}^{\pi} F_{11}(\theta)\sin(\theta)\,d\theta} \tag{2}$$

is calculated, where $F_{11}(\theta)$ is the phase function. This is not to be mistaken as the backscattering cross section or the backscattering fraction for isotropically incident radiation. This angle integration was calculated by using the expansion of the phase function in Legendre polynomials:

$$F_{11}(\theta) = \sum_{s=0}^{\infty} a_s P_s(\cos\,\theta). \tag{3}$$

By using the integration properties of the Legendre polynomials, Q_{back} can be expressed as

$$Q_{back} = \frac{1}{2}\left(a_0 + \sum_{\substack{s=1 \\ s\ \text{odd}}} a_s I_s\right), \quad \text{where } I_1 = -\frac{1}{2},\ \ I_s = -\frac{s-2}{s+1} I_{s-2}. \tag{4}$$

In order to comply with the terminology and symbols recommended by the International Association for the Physical Science of the Oceans (IAPSO), optical properties are also specified in terms of the wavelength-dependent absorption, scattering, and extinction coefficients, respectively, $a(\lambda), b(\lambda), c(\lambda)$, expressed in m^{-1} [25]. For a monochromatic collimated beam crossing an infinitesimally thin layer of the medium normal to the beam, the absorption coefficient, $a(\lambda)$, is defined as $-d\Phi_a/\Phi dr$, where dr is the thickness of the layer, Φ is the incident flux, and $d\Phi_a$ is the flux lost by means of absorption. Likewise, the scattering coefficient $b(\lambda)$ is defined as $-d\Phi_b/\Phi dr$, where $d\Phi_b$ is the flux scattered from the beam. The attenuation coefficient can be obtained as the sum of $a(\lambda)$ and $b(\lambda)$. For a monodisperse solution of N particles per unit volume, the absorption coefficient $a(\lambda)$ is linked to C_{abs} by the relation $a(\lambda) = NC_{abs}$; likewise for $b(\lambda)$, $c(\lambda)$. A backscattering coefficient can also be defined as $b_b(\lambda) = NQ_{back}C_{sca}$. In the case of a polydisperse population of particles, cross sections have to be size-averaged: $a(\lambda) = N\langle C_{abs}\rangle$, $b(\lambda) = N\langle C_{sca}\rangle$, $c(\lambda) = N\langle C_{ext}\rangle$, $b_b(\lambda) = N\langle Q_{back}C_{sca}\rangle$.

4. Results and discussion

Light-scattering properties were calculated for homogeneous and coated spheres and spheroids, and the results were averaged on size according to the experimentally determined particle size distribution given in Fig. 3. Electron microscopy data suggests a spheroidal axial ratio $\varepsilon = 0.7$ (prolate). In both spherical and

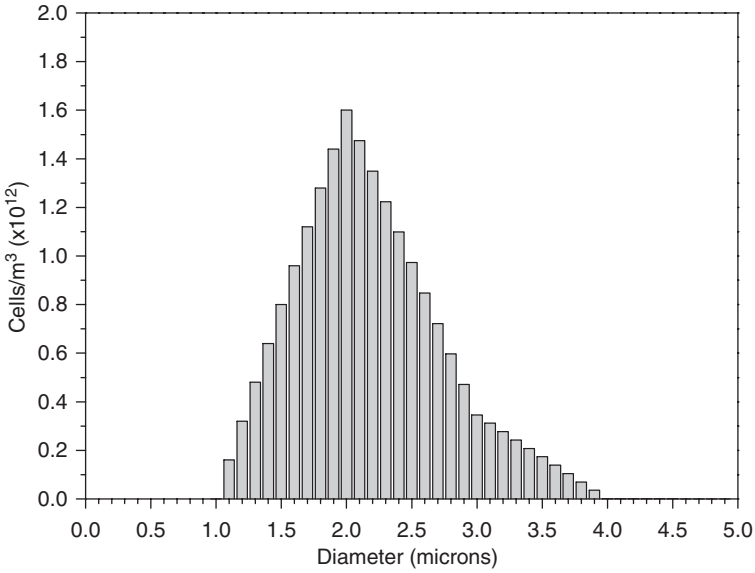

Fig. 3. Particle size distribution for *Aureococcus anophagefferens* (South African West Coast, January 2004 bloom).

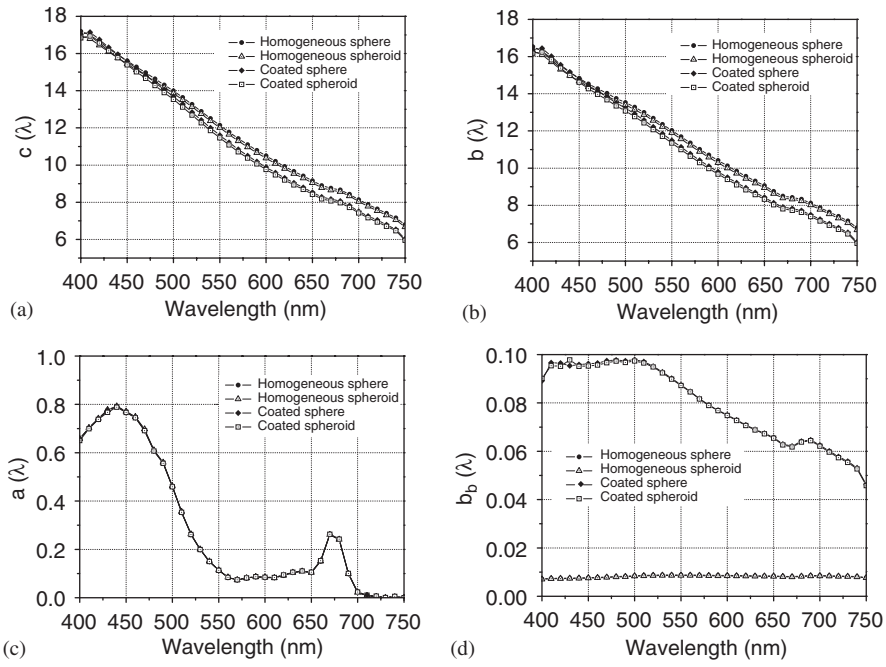

Fig. 4. Extinction, scattering, absorption, and backscattering values calculated for the particle size distribution of Fig. 3 and index of refraction values as given by Fig. 2. Core/particle ratio is set to $q = 0.9472$ for coated spheres and spheroids. For homogeneous and coated spheroids, axial ratio is $\varepsilon = 0.7$.

spheroidal case, the core/particle ratio was set as $q = 0.9472$, which yields a 0.15 shell volume fraction, and a chloroplast coating was used. Extinction, scattering, absorption and backscattering coefficients can be seen in Figs. 4a–d.

All four shapes (homogenous and coated spheres, homogeneous and coated spheroids) yield similar values of the scattering and absorption coefficient. The differences due to particle composition (homogeneous vs.

coated) are larger than those due to shape (spheres vs. spheroids). Attenuation and scattering values are slightly larger at higher wavelengths for homogeneous particles. In the case of absorption, plots almost overlap each other, thus suggesting that the retrieval of refractive indices does not require nonspherical particle models (EBCM), and therefore the use of exact, spherical models (either Mie for homogeneous spheres or Aden–Kerker for coated spheres) suffice for that purpose.

The effect of particle structure on backscattering is more noticeable. A two-layered size distribution of particles show backscattering coefficient values for coated scatterers which are between 5 and 10 times higher than those for homogeneous particle values. While backscattering seems to be shape-independent, as Fig. 4d apparently show for coated spheres and spheroids, this is an effect of size averaging. Fig. 5 shows backscattering probability factor values Q_{back} for coated spheres with 1000–5000 nm equivalent-volume-sphere diameter values and a single wavelength value of $\lambda = 570\,\mathrm{nm}$. Differences between spheres and spheroids range from 0% to 23% for Q_{back}, while scattering cross section values change by less than 1.5%. When size-averaged, backscattering coefficient values b_{b} are found to be $0.08183\,\mathrm{m}^{-1}$ for coated spheres and $0.08167\,\mathrm{m}^{-1}$ for coated spheroids, a mere 0.2% difference. Prior calculations made for coated particles (both spherical and spheroidal) with a chloroplast core and a cytoplasm shell show that backscattering values are similar to those of homogeneous scatterers. This comes as evidence that backscattering is heavily dependent not only on particle composition, but also on how chloroplast—the more absorbing material—is located in the cell.

In order to assess the validity of this hypothesis in real-life situations, reflectance measurements were used. Remote sensing reflectance R_{rs} (the light leaving the sea surface normalised to the incident light), can be expressed in the reflectance approximation in terms of the absorption and backscattering properties of the water column [26]:

$$R_{\mathrm{rs}}(\lambda) = \frac{L_{\mathrm{u}}(0^+,\lambda)}{E_{\mathrm{d}}(0^+,\lambda)} \approx \frac{f}{Q}\,\frac{b_{\mathrm{bt}}(\lambda)}{a_{\mathrm{t}}(\lambda) + b_{\mathrm{bt}}(\lambda)}, \tag{5}$$

where $L_{\mathrm{u}}\,(0^+,\lambda)$ is the upwelling radiance just above the sea surface, $E_{\mathrm{d}}\,(0^+,\lambda)$ is the downwelling irradiance just above the sea surface, f/Q is an assumed constant ($= 0.085$) describing the angular structure of the light field, and $a_{\mathrm{t}}(\lambda)$ and $b_{\mathrm{bt}}(\lambda)$ are the total absorption and backscattering coefficients, respectively.

Whilst it is not possible to provide absolute validation of the various model geometries presented here, due to the lack of angular scattering data, the reflectance approximation does allow indirect validation, providing

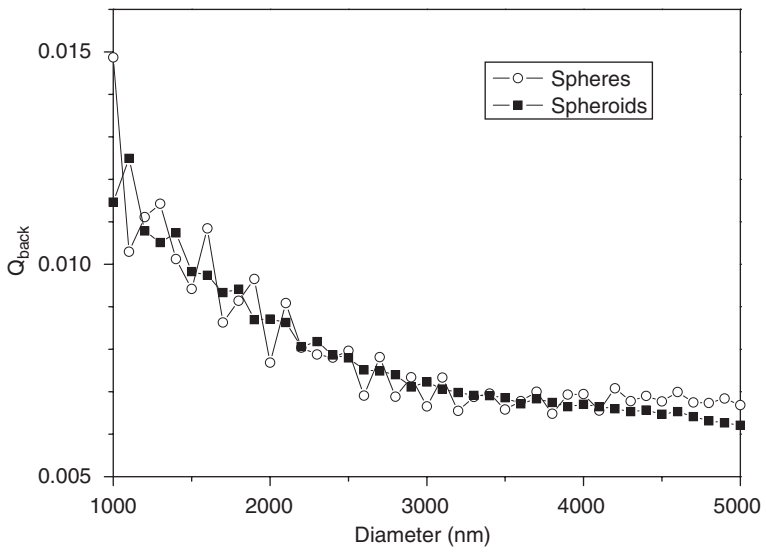

Fig. 5. Backscattering probability factor values Q_{back} for monodisperse, coated spheres (circles) and coated spheroids (squares) with refractive index values $m_{\mathrm{core}} = 1.0351 + \mathrm{i}7.624{*}10^{-5}$ and $m_{\mathrm{shell}} = 1.1415 + \mathrm{i}7.452{*}10^{-4}$, and a core/particle ratio $q = 0.9472$.

absorption and backscattering data for all the water constituents are known. The approach does offer several other advantages. Firstly, one of the primary reasons for studying algal backscattering is the potential effect on ocean colour; the reflectance approximation provides a relatively simple means of achieving this. In addition, it is the backscattering coefficient (the angular scattering integrated in the backward direction) that is more immediately important to ocean colour studies than the phase (or volume scattering) function: the reflectance approximation allows simple validation of backscattering rather than the considerably more complex validation of the whole phase function.

Briefly, the modelled algal absorption and backscattering data from the various geometries are used as input to Eq. (5). Input for other constituents are derived from measurement and the literature. Detrital and dissolved (an operational definition of $<0.7\,\mu m$) absorption are from direct measurement, as discussed above. Detrital backscattering is calculated by fractionating the total particulate scattering from the AC-9 instrument into algal and detrital components, as determined from the measured a_ϕ/a_d ratio. A spectrally flat backscattering probability of 0.1% was then assumed—the lower end of values suggested by Morel et al. [27]. The backscattering of small particles (e.g. bacteria and lithogenic particles) associated with the dissolved fraction was calculated from the measured scattering of this fraction, assuming a backscattering probability of 1%. The absorption of water was given by the data of Pope and Fry [28], and pure seawater backscattering coefficients by Morel [29].

Reflectance measurements were taken from the *A. anophagefferens* January 2004 bloom, and results were compared to those obtained from Mie, Aden–Kerker and EBCM calculations. As Fig. 6 show, Mie calculations underestimate the value of reflectance by a factor of 3. When coated particles with a cytoplasm core and a chloroplast coating are considered, reflectance calculated values fit better the expected experimental values. This better fit is due to the assumption of coated particles with absorbing shell, which yield a much larger contribution to total backscattering than homogeneous particles (Fig. 4d). In our comparison, Aureococcus account for 75–80% of the entire backscattering. While it must be remembered that we are dealing with a very specific algal bloom, our findings agree with previous Mie-based assessments showing that the known seawater constituents are unable to account for the observed brightness of the ocean [30]. It is reasonable to assume that Mie backscattering underestimations have lead to an overestimation of the "missing" backscattering [8], and therefore the use of heterogeneous models can help find a significant portion of the missing backscattering [31].

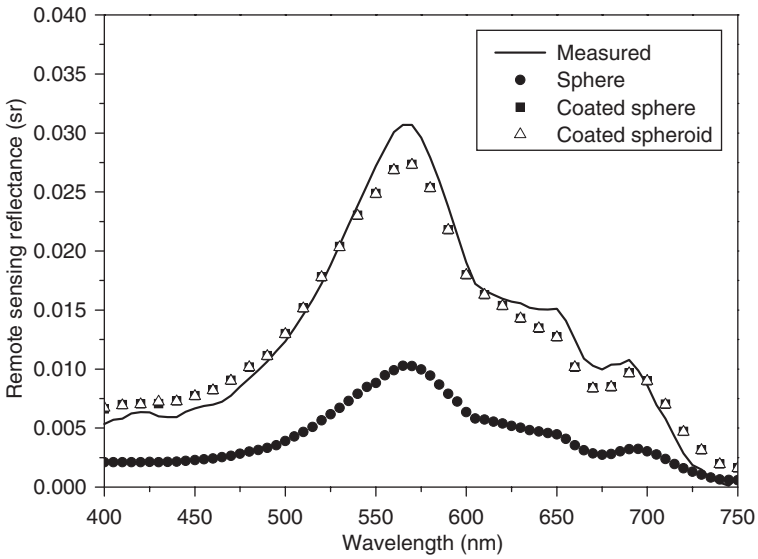

Fig. 6. Remote-sensing reflectance $R_{rs}(\lambda)$ experimental values (full line) and calculated values for the particle size distribution of Fig. 3 and for index of refraction values as given by Fig. 2, for homogeneous spheres (circles), coated spheres (black squares) and coated spheroids (white squares). For coated particles, $q = 0.9472$. For homogeneous and coated spheroids, axial ratio is $\varepsilon = 0.7$.

The coincidence between calculated reflectance data for coated spheres and coated spheroids (less than 1% variation at all wavelengths, and a mere 0.1% change in the region of largest brightness) comes as a surprise, as backscattering data is usually found to be dependent on particle shape. As already explained, however, this seems to be an effect of polydispersity. Should this be a general case, Aden–Kerker theory would suffice to improve theory–experiment fits in oceanographic light-scattering studies where particles with a size range of a few microns are considered. Whether this is the case for any particle size distribution is, however, an open question.

Acknowledgements

Financial support from project MAT2004-00866 (Ministry of Science and Technology, Spain; FEDER Funds, EU) is acknowledged.

References

[1] Preisendorfer RW. Hydrologic optics, vol. 5. Properties. USA: US Environmental Research Laboratories; 1976.
[2] Morel A, Prieur L. Analysis of variations in ocean color. Limnol Oceanogr 1977;22:709–22.
[3] Bricaud A, Morel A. Light attenuation and scattering by phytoplanktonic cells: a theoretical modeling. Appl Opt 1986;25:571–80.
[4] Stramski D, Bricaud A, Morel A. Modeling the inherent optical properties of the ocean based on the detailed composition of planktonic community. Appl Opt 2001;40:2929–45.
[5] van de Hulst HC. Light scattering by small particles. New York: Wiley; 1957.
[6] Quinby-Hunt MS, Hunt AJ, Lofftus K, Shapiro D. Polarized-light scattering studies of marine Chlorella. Limnol Oceanogr 1989;34:1587–600.
[7] Volten H, de Haan JF, Hovenier JW, Schreurs R, Vassen W, Dekker AG, et al. Laboratory measurements of angular distributions of light scattered by phytoplankton and silt. Limnol Oceanogr 1998;43:1180–97.
[8] Stramski D, Boss E, Bogucki D, Voss KJ. The role of seawater constituents in light backscattering in the ocean. Progr Oceanogr 2004;61:27–56.
[9] Yentsch CS. Measurement of visible light absorption by particulate matter in the ocean. Limnol Oceanogr 1962;7:207–17.
[10] Roesler CS. Theoretical and experimental approaches to improve the accuracy of particulate absorption coefficients derived from the quantitative filter technique. Limnol Oceanogr 1998;43:1649–60.
[11] Kishino M, Takahashi M, Okami N, Ichimura S. Estimation of the spectral absorption coefficients of phytoplankton in the sea. Bull Mar Sci 1985;37:634–42.
[12] Albert A, Mobley CD. An analytical model for subsurface irradiance and remote sensing reflectance in deep and shallow case-2 waters. Opt Express 2003;11:2873–90.
[13] WETLabs. AC-9 protocol document, revision D. Philomath, OR: Western Environmental Technology Laboratories (WETLabs); 2000.
[14] Bernard S, Probyn TA, Barlow RG. Measured and modelled optical properties of particulate matter in the southern Benguela. S Afr J Sci 2001;97(9–10):410–20.
[15] Toon OB, Ackerman TP. Algorithms for the calculation of scattering by stratified spheres. Appl Opt 1981;20:3657–60.
[16] Stephens FC. Variability of spectral absorption efficiency within living cells of *Pyrocystis lunula* (Dinophyta). Mar Biol 1995;122:325–31.
[17] Paillotin G, Leibl W, Gapinski J, Breton J, Dobek A. Light gradients in spherical photosynthetic vesicles. Biophys J 1998;75:124–33.
[18] Kleima FJ, Hofmann E, Gobets B, van Stokkum IHM, van Grondelle R, Diederichs K, et al. Forster excitation energy transfer in peridinin-chlorophyll-*a*-protein. Biophys J 2000;78:344–53.
[19] Morel A, Bricaud A. Inherent properties of algal cells including picoplankton: theoretical and experimental results. In: Platt T, Li WKW, editors. Photosynthetic picoplankton, Can Bull Fish Aq Sci 1986;214:521–59.
[20] Bohren CF, Huffman DR. Absorption and scattering of light by small particles. New York: Wiley; 1983.
[21] Waterman PC. Symmetry, unitarity, and geometry in electromagnetic scattering. Phys Rev D 1971;3:825–39.
[22] Mishchenko MI. Light scattering by randomly oriented axially symmetric particles. J Opt Soc Am A 1991;8:871–82 Errata 1992;9:497.
[23] Peterson B, Ström S. T-matrix formulation of electromagnetic scattering from multilayered scatterers. Phys Rev D 1974;10:2670–84.
[24] Quirantes A. A T-matrix method and computer code for randomly oriented, axially symmetric coated scatterers. JQSRT 2005;92:373–81.
[25] Morel A, Smith RC. Terminology and units in optical oceanography. Mar Geod 1982;5:335–49.
[26] Zaneveld JRV. A theoretical derivation of the dependence of the remotely sensed reflectance on the inherent optical properties. J Geophys Res 1995;100(C7):13,135–42.
[27] Morel A, Antoine D, Gentili B. Bidirectional reflectance of oceanic waters: accounting for Raman emission and varying particle phase function. Appl Opt 2002;41:6289–306.

[28] Pope RM, Fry ES. Absorption spectrum (380–700 nm) of pure water. II. Integrating cavity measurements. Appl Opt 1997;36: 8710–23.
[29] Morel A. Optical properties of pure water and pure seawater. In: Jerlov, Steeman Nielsen E, editors. Optical aspects of oceanography. New York: Academic; 1974. p. 1–24.
[30] Morel A, Ahn YH. Optics of heterotrophic nanoflagellates and ciliates: a tentative assessment of their scattering role in oceanic waters compared to those of bacterial and algal cells. J Mar Res 1991;49:177–202.
[31] Zaneveld JRV, Kitchen JC. The variation in the inherent optical properties of phytoplankton near an absorption peak as determined by various models of cell structure. J Geophys Res 1995;100(C7):13,309–20.